ACSNANO
www.acsnano.org
ARTICLE

Dynamic Behavior of the Triboelectric Charges and Structural Optimization of the Friction Layer for a Triboelectric Nanogenerator

Nuanyang Cui,[†,‡] Long Gu,[§] Yimin Lei,[†,‡] Jinmei Liu,[§] Yong Qin,[§] Xiaohua Ma,[*,†,‡] Yue Hao,[*,†,‡] and Zhong Lin Wang[∥]

[†]School of Advanced Materials and Nanotechnology and [‡]Wide Bandgap Semiconductor Technology Disciplines State Key Laboratory, Xidian University, Xi'an 710071, China

[§]Institute of Nanoscience and Nanotechnology, Lanzhou University, Lanzhou 730000, China

[∥]School of Material Science and Engineering, Georgia Institute of Technology, Atlanta, Georgia 30332, United States

Supporting Information

ABSTRACT: Seeking to increase the triboelectric charge density on a friction layer is one of the most basic approaches to improve the output performance of triboelectric nanogenerators (TENGs). Here, we studied the storage mechanism of triboelectric charge in the friction layer and discussed the function of carrier mobility and concentration in the charge-storing process. As guided by these results, a kind of composite structure is constructed in the friction layer to adjust the depth distribution of the triboelectric charges and improve the output performance of TENGs. To further elucidate this theory, a simple TENG, whose negative friction layer is a composite structure by integrating polystyrene (PS) and carbon nanotubes (CNTs) into polyvinylidene fluoride (PVDF), was fabricated, and its performance test was also carried out. Comparing with a pure PVDF friction layer, the composite friction layer can raise the triboelectric charge density by a factor of 11.2. The extended residence time of electrons in the friction layer is attributed to a large sum of electron trap levels from PS.

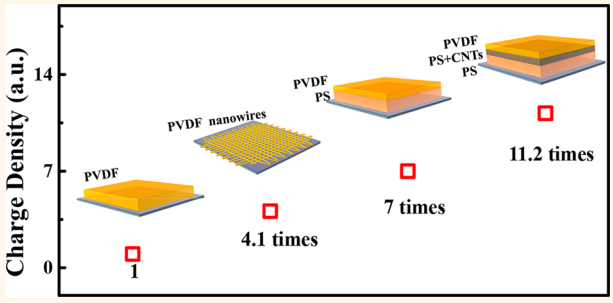

KEYWORDS: *triboelectrification, nanogenerator, composite friction layer, triboelectric charge, charge storage*

Recently, the triboelectric nanogenerator (TENG) based on coupling of a triboelectric effect and electrostatic induction has been extensively developed for harvesting mechanical energy from ambient environment.[1] Unlike a traditional chemical battery with limited lifespan[2] and the need for frequent replacement or recharging, a TENG can directly translate mechanical energy into electrical energy and power the functional electronics instantly. Although many other approaches based on different mechanisms have been demonstrated for effectively harvesting mechanical energy, such as piezoelectric nanogenerators,[3−12] electromagnetic generators,[13,14] and electrostatic generators,[15] TENGs are more dominant in power output and energy conversion efficiency.[16−18] This makes TENGs most likely to be the energy supply for portable electronics[19−21] and even possibly to be used for large-scale power generation in the near future.

The working process of TENGs can be basically divided into two steps: separation process of positive and negative charges caused by friction or contact and an electricity output process induced by electrostatic induction. The latter step is mainly related to the device structure design, which usually focuses on solving the problem of the device's adaptability in different environments.[22−24] The first step, however, is mostly important for the output of TENG because both the current and voltage output are proportional to the triboelectric charge density on the friction layer. Research in recent years suggested that matching appropriate materials and building surface microstructure can greatly increase the triboelectric charge density and the output of a TENG.[25−27] However, these results are either experimental outcomes or simple, qualitative theoretical analyses. Limited research is available about the fundamental mechanism of the triboelectrification process. Therefore, we have no definite guidelines on how to effectively adjust the triboelectric charge density in the friction layer.

Actually, the triboelectrification process can be further divided into three subprocesses: the generation of the triboelectric charges, the storage of the charges, and the loss

Received: March 25, 2016
Accepted: April 29, 2016

DOI: 10.1021/acsnano.6b02076
ACS Nano XXXX, XXX, XXX−XXX

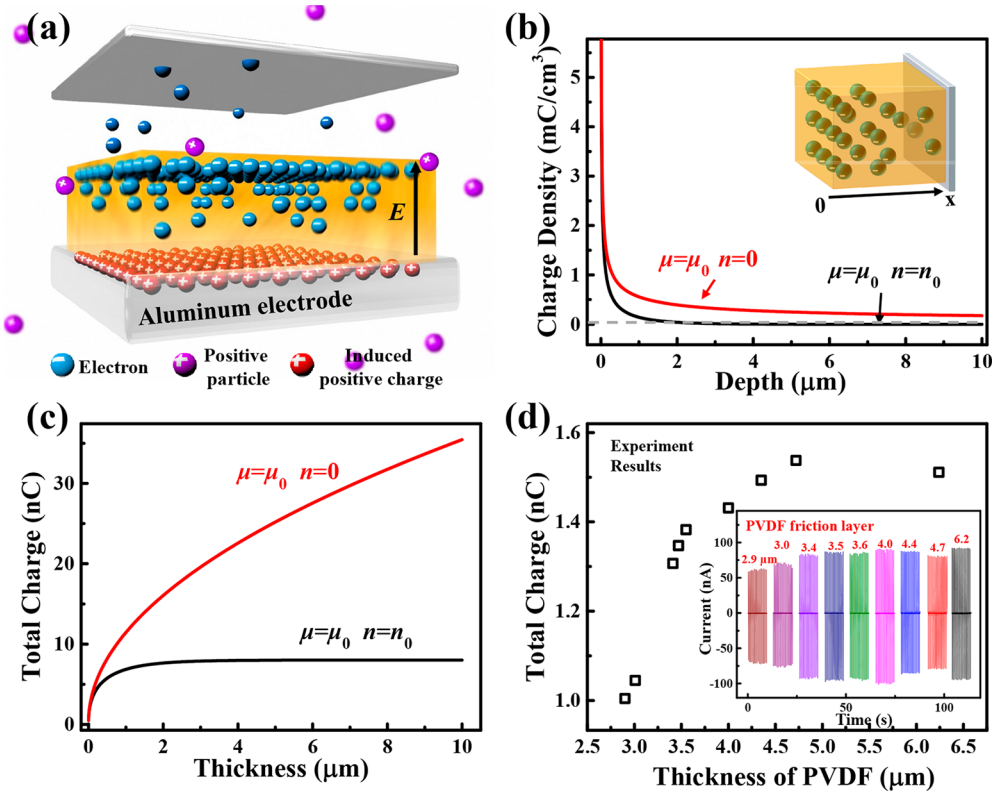

Figure 1. (a) Schematic of the transport process of triboelectric electrons in the negative friction layer of a TENG. (b) Theoretical triboelectric charge distribution in the friction layer. The red line is the result of only taking the carrier mobility μ_0 into account, and the black line is the result considering both carrier mobility μ_0 and its intrinsic carrier density n_0. (c) Theoretical relationship between the total storage charge and the thickness of the friction layer. (d) Measured total surface charge in the PVDF friction layer with different thicknesses. The corresponding short-circuit currents are shown in the inset.

of the charge, respectively. First, it is only possible to know the tendency of materials to gain or lose electrons based on the triboelectric series, but the issues of most concern are the exact yield of triboelectric charges (TCY) in a certain condition as well as its influence factor and extent. Second, after the positive and negative charges are separated, the storage position of triboelectric charges still needs to be considered. Third, our previous experiments indicated that the triboelectric charge stored in the friction layer will decay along with time. However, the factors that affect the process and the influence degree are still mysteries until now. If all of these problems can be figured out, the performance of TENGs can be further improved.

In this work, the relationship between the friction layer thickness and the transport process of triboelectric charges in a polyvinylidene fluoride (PVDF) film are investigated in detail. It is noticed that if the thickness of the friction layer is larger than the storage depth, the stored charge can reach a maximum, and the excess increase of the storage depth does not contribute to the charge accumulation. More importantly, based on the calculated results, a dielectric layer and a transport layer were added between the PVDF layer and the electrode. This multilayer structure design provided a factor of 11.2 improvement for the output performance of the TENG. As a general conclusion, the study of the transport process of triboelectric charges in the friction layer provides a new efficient approach to guide our work in TENG research.

RESULTS AND DISCUSSION

Monolayer Friction Layer. First, a model for the generation, transport, and loss process of the triboelectric charge was established. As seen in Figure 1a, the orange part represents the negative friction layer, which will capture electrons from the positive friction layer (top aluminum electrode in Figure 1a) during the triboelectrification process. As the electrons are accumulated on the contact surface, the positive charges can be induced into the electrode. As shown in the schematic, an electric field will be set up between the contact surface and electrode, and the electric field direction is vertically upward. Therefore, two electron transfer modes exist: a drift process caused by the electric field and a diffusion process caused by the concentration gradient of electrons. The loss of the triboelectric electrons comes from two aspects: one is adsorbing positively charged ions or particles from air and the other one is the combination with the induced positive charges on the electrode. In order to simplify the calculation, several assumptions should be put forward:

(1) When the driving force is constant, the TCY is also constant for a moment.
(2) Considering the actual electric field intensity is large enough in our experiment, the diffusion process can be neglected.
(3) We take into account only the charge loss caused by the combination of electrons and the induced positive charges on the electrode.
(4) We neglect the impact of the trap levels on the triboelectric electrons temporarily.

DOI: 10.1021/acsnano.6b02076
ACS Nano XXXX, XXX, XXX−XXX

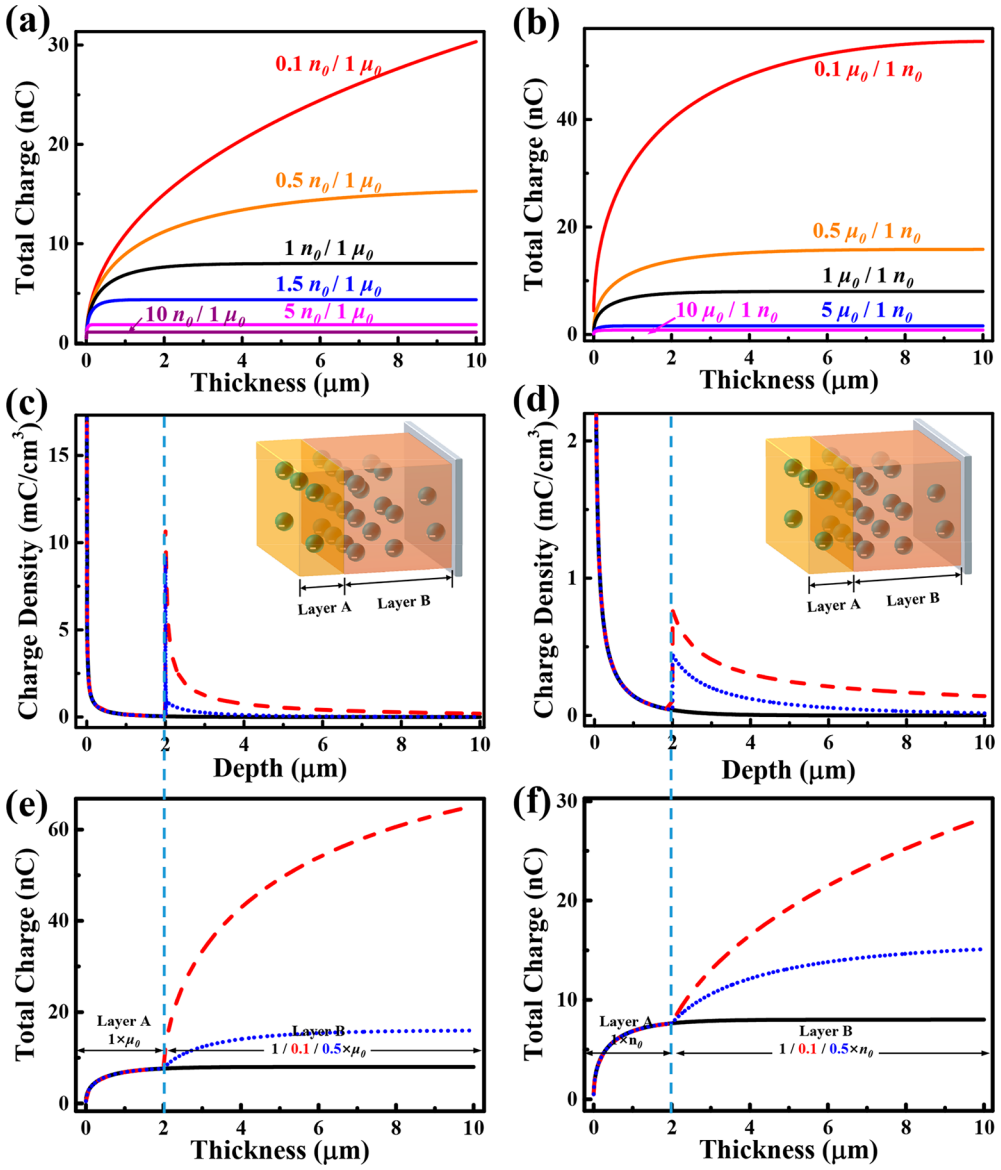

Figure 2. (a and b) Theoretical relationship between the total storage charge and the thickness of the friction layer with different carrier mobility and intrinsic carrier density. (c and d) Theoretical triboelectric charge distribution in the bistratal friction layer. (e and f) Theoretical relationship between the total storage charge and the thickness of the bistratal friction layer.

(5) Compared with the sample thickness, the area of the contact surface is large enough that the sample can be assumed as one-dimensional.

Under the above assumptions the electron drift process is modeled by the drift equation and solved by the recursion method. The details are shown in the Supporting Information.

As PVDF is one of the most commonly used negative materials for TENGs, it will be the major research subject in this work. The carrier mobility and intrinsic carrier density of PVDF are $\mu_0 = 1.2 \times 10^{-10}$ cm^2/V·s and $n_0 = 5.5 \times 10^{16}$ cm^{-3}, respectively. The contact surface area is about 1 cm^2. The TCY is approximately equal to 0.1 nC/s (this is an average value measured within 10 s after the TENG begins to work, taken from our following experimental test, shown in Figure 6). Figure 1b shows the theoretical triboelectric charge distribution through the depth of the friction layer under enough friction time. The red line is the result with only the PVDF carrier mobility being taken into account, and the black line is the result when considering both PVDF carrier mobility and its intrinsic carrier density. Accounting for the carrier mobility solely, the triboelectric charge density will decrease with an increase in the depth of the PVDF layer but never reach zero. Considering the relationship between total quantity of the triboelectric charge and the thickness of the PVDF layer (Figure 1c), it is noticed that the thicker the friction layer, the more triboelectric charge that will be obtained. Actually, the intrinsic carriers in PVDF can promote the combination of the triboelectric electrons, leading to the conversion of triboelectric charge density to zero quickly in the friction layer (black line in Figure 1b). When the PVDF thickness reaches about 4 μm, there is a maximum value for the total charge amount stored in the PVDF layer, and the excess thickness does not contribute to the charge accumulation.

To verify the calculated results through experiments, nine TENGs were fabricated, in which the negative friction layers are PVDF films with different thicknesses prepared by spin-coating and the positive friction layers are all aluminum foil. With

DOI: 10.1021/acsnano.6b02076
ACS Nano XXXX, XXX, XXX−XXX

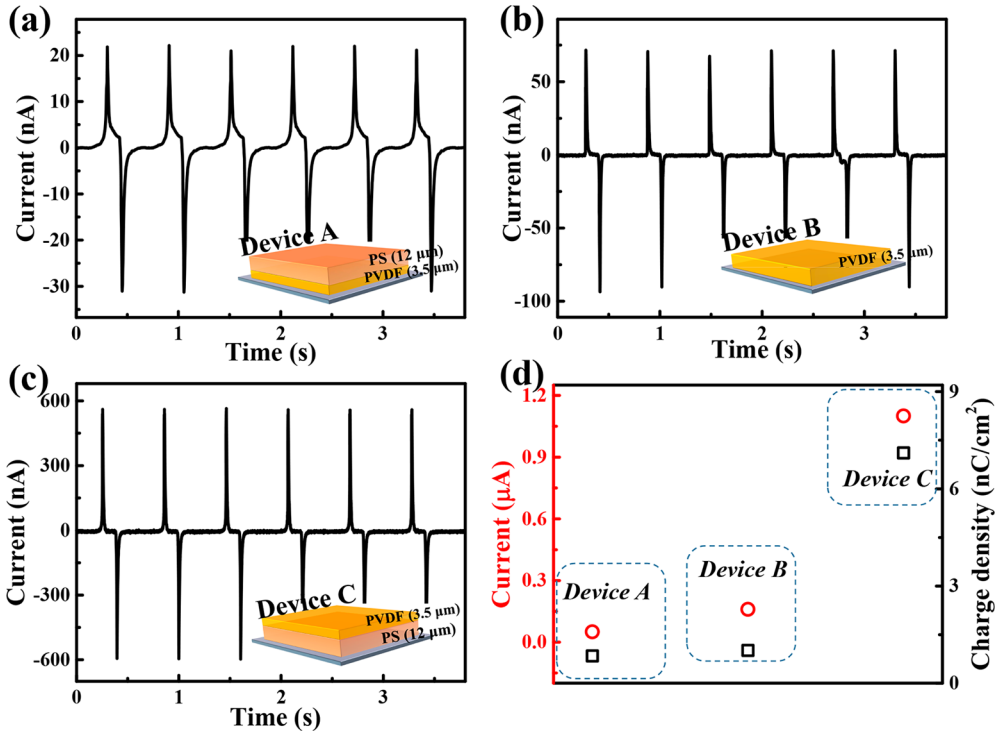

Figure 3. Short currents of device A (a), device B (b), and device C (c). Device A has a 12 μm thick PS friction layer and 3.5 μm thick PVDF dielectric layer; device B has a 3.5 μm thick PVDF friction layer only, and device C has a 3.5 μm thick PVDF friction layer and 12 μm thick PS dielectric layer. (d) Peak currents and total surface charge of these three devices.

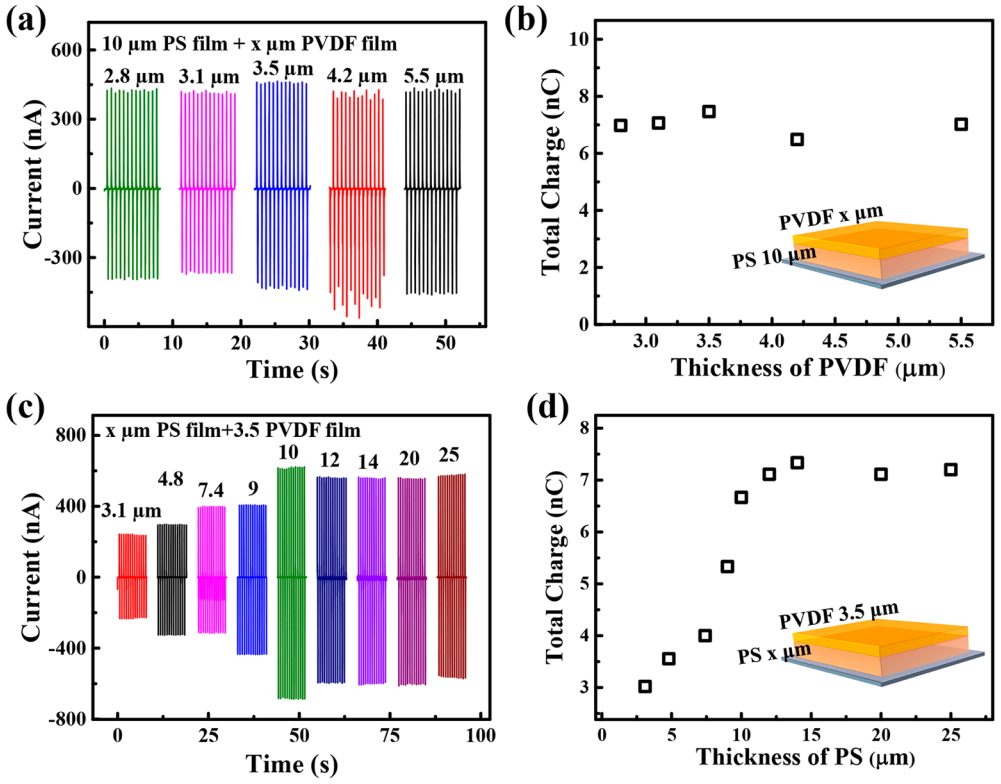

Figure 4. Short currents (a) and total surface charge of a TENG with different thickness PVDF friction layers and a PS dielectric layer of 10 μm thickness. Short-circuit currents (c) and total surface charge of a TENG with different thickness PS dielectric layers and a PVDF friction layer of 3.5 μm thickness.

preparatory work completed, these TENGs were set to work for 30 min under the same driving condition. The short-circuit current of these devices was collected and are shown in the inset of Figure 1d. Figure 1d shows the change rule of the areal

DOI: 10.1021/acsnano.6b02076
ACS Nano XXXX, XXX, XXX−XXX

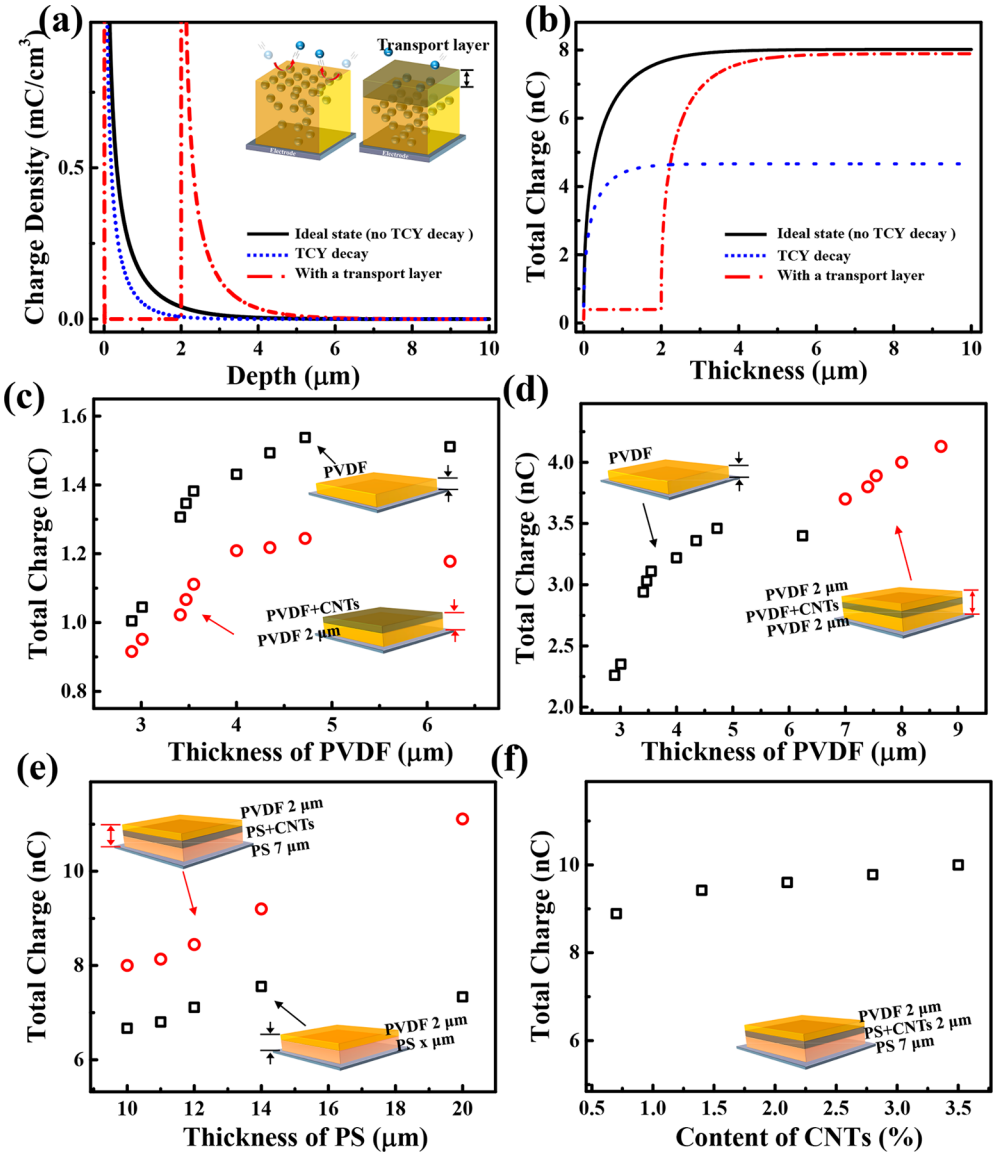

Figure 5. (a) Theoretical triboelectric charge distribution in the friction layer for three different states: ideal states (no TCY decay) (black line), considering the TCY decay (blue dotted line), and adding a transport layer on the surface (red dot-dashed line). (b) Theoretical relationship between the total storage charge and the thickness of the friction layer for the three different states. (c–f) Measured total surface charge in the friction layer of TENGs with different structures.

density of the total triboelectric charge with the increase of the PVDF layer thickness. Similar to the theoretical calculation, the triboelectric charge areal density in the PVDF layer increases with increasing its thickness at the beginning and then reaches a stable status. In the calculation process above, the theoretical model has been simplified, leading to the deviation of the results from the experimental outcomes. However, from their similar variation trend, a further understanding of the triboelectric charge transport and storage processes can be obtained. Further analysis about the effect of the carrier mobility and intrinsic carrier density on the storage of triboelectric charge has been carried out, as shown in Figure 2. It is noticed that the triboelectric charge distribution changes with adjusting these two parameters independently, as shown in Figure S2. When the carrier mobility is reduced to 10%, the total amount of the triboelectric charge stored in the PVDF layer is increased about 7 times (Figure 2a). Then on reducing the intrinsic carrier density, the storage depth is obviously increased while the incremental amount of the triboelectric charge is less than that in reducing the carrier mobility. This means that a smaller intrinsic carrier density can significantly increase the valid thickness of the friction layer (Figure 2b). Therefore, an ideal material for TENG needs to have a larger TCY, smaller carrier mobility, as well and smaller intrinsic carrier density, but these requirements can hardly be met simultaneously.

Double-Layer Composite Friction Layer. To assemble the advantages of different materials into one, a composite structure model is attempted to be established for the friction layer. First, layer A is selected as the contact surface, whose mobility and intrinsic carrier density are μ_0 and n_0, respectively. Then a thick dielectric layer, layer B, is added between layer A and the electrode. This dielectric layer should have a smaller carrier mobility or smaller intrinsic carrier density. The simulation calculation results are shown in Figure 2c–f. It is proved theoretically that a composite layered structure can

DOI: 10.1021/acsnano.6b02076
ACS Nano XXXX, XXX, XXX–XXX

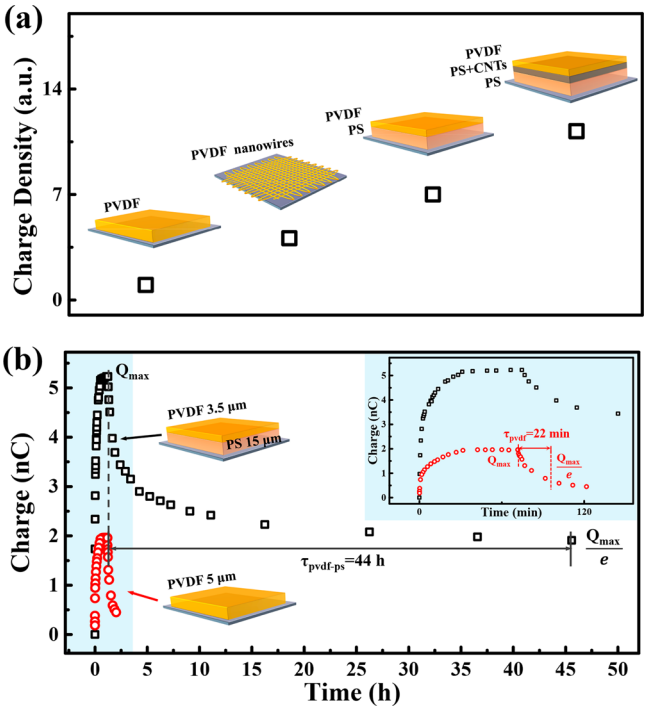

Figure 6. (a) Improvement effects of different composite friction layer structure. (b) Accumulation process and decay process of the triboelectric charge for a pure PVDF TENG device (red circle) and a PVDF-PS TENG device (black square).

improve the total storage charge and storage depth dramatically. To verify the feasibility of this method, TENG devices were prepared accordingly: device A has a PS friction layer with a thickness of 12 μm and a PVDF dielectric layer with a thickness of 3.5 μm. Device B has only a PVDF friction layer with a thickness of 3.5 μm, while device C has a PVDF friction layer with a thickness of 3.5 μm and a 12 μm PS dielectric layer. The positive friction layers of these TENG devices are all aluminum foils. After making these TENGs work for 30 min under the same driving conditions, the short-circuit current of these devices are collected respectively, as shown in Figure 3a–c. Figure 3d illustrates the current peak values and the surface charge density of the three devices. Compared with PVDF, PS is not an ideal negative friction material for TENG due to its weaker ability to capture electrons from the positive friction layer; thus both the current peak and surface charge density of device A are smaller than those of device B. The intrinsic carrier density of PS is smaller than that of PVDF, and the electron mobility of PS is also smaller than that of PVDF because PS has abundant trap levels of electrons. These make PS one of the most suitable dielectric materials. TENG device C, with the PS dielectric layer, shows an amazing charge storage ability that is 7 times as much as that in device B, with the pure PVDF layer. To investigate the effect of the PVDF–PS composite structure in depth, we prepared two groups of new TENG devices. One group has a varied thickness of the PVDF friction layer while keeping the PS layer the same. The other group has a varied thickness of the PS dielectric layer while keeping the PVDF layer the same. With preparatory work completed, the outputs of these devices were obtained, respectively. Figure 4a is the short-circuit currents of devices in group 1, and Figure 4b shows the surface total charge accumulated in the composite layer. Unlike the situation in Figure 1d, the thickness variation of the PVDF layer does not have a significant influence on the stored charges. From the above results it can be surmised that most of the triboelectric charges are stored in the PS dielectric layer, and this is soon confirmed by the test results of devices in group 2 (Figure 4 c and d). As the thickness of the PS layer was increased from 3.1 μm to 14 μm, the accumulated charge increases from 3 nC/cm^2 to 7.3 nC/cm^2 and then reaches a stable status. This trend is completely consistent with the pure PVDF device (Figure 1d) and the theoretical results (Figure 2c and d).

Three-Layer Composite Friction Layer. Although the experimental result is well consistent with the calculated result in the variation trend of triboelectric charges, there exists a great gap between the total charge quantity of these two results. With a pure PVDF device, for example, the calculated value of the maximal stored charge is 8 nC/cm^2, but the experimental result is only 1.5 nC/cm^2. In our opinion, this gap probably comes from the simplification of the theoretical model. The two most important points can be summarized as the combination of triboelectric charge and ions or charged particles in the air as well as the impact of the TCY. At present, only the second point is addressed in this study. In the previous calculation, the TCY is simply regarded as a constant. However, the triboelectric charge that enters the friction layer early would in turn block the entrance of other charges, as shown in the left inset in Figure 5a. In this way, the TCY will decrease gradually with the accumulation of triboelectric charges. If there really exists an attenuation effect on the TCY, the most important factors must be the quantity of triboelectric charge and the distance between the contact surface and the charge. The more the charges are accumulated, the smaller the TCY. Also, the shallower the storage depth of charges, the smaller the TCY. In order to solve the problem theoretically, two assumptions should be put forward:

(1) Only the charge stored at a depth of 0 to 2 μm affects the TCY, and all of these charges have the same impact degree on the TCY.
(2) Along with the increase of the accumulated charge, the TCY tends to decay exponentially. The attenuation function can be described as

$$I_c = a \times \exp(-q/A) \quad (1)$$

Here I_c is the actual TCY, a is the ideal maximum TCY, q is the total charge quantity accumulated at a depth from 0 to 2 μm, and A is an attenuation coefficient. When considering the attenuation of TCY, the new calculated results (blue line in Figure 5a and b) are significantly smaller than the early results (black line in Figure 5a and b). The most important thing to the TENG is its output performance. However, now the charges close to the contact surface will restrain the entering of new charges; thus a method to lead the superficial charges to a deep position should be found. On the basis of the above analysis, we can replace a thin layer on the very surface with a new transport layer that has a high conductivity. In this way, the accumulated charge in the top surface layer will become less, and accordingly the attenuation effect on TCY will also be weakened; the schematic is shown in the right inset in Figure 5a. The red lines in Figure 5a and b are the calculated results when the carrier mobility and intrinsic carrier density of the surface layer of a thickness of 2 μm decreased by 5 times compared with the original value. The red line in Figure 5b obviously shows that this adjustment is very effective.

DOI: 10.1021/acsnano.6b02076
ACS Nano XXXX, XXX, XXX–XXX

To form the transport layer mentioned above in the following experiments, 0.7 wt % carbon nanotubes (CNTs) were added into PVDF or PS. This transport layer should be sandwiched between the friction layer and the dielectric layer rather than put on the outermost layer; if not, triboelectric charges will be lost through the transport layer. As shown in Figure 5c, when the transport layer is put on the outermost layer, the total accumulated charge (red point) is less than that in the pure PVDF device (black point). If this transport layer is added between two PVDF layers, the charge density in the composite layer is improved significantly and is even larger than the maximum charge density of the pure PVDF device, as shown in Figure 5d. For the PVDF−PS composite layer device, the transport layer, which is composed of 99.3 wt % PS and 0.7 wt % CNTs, was sandwiched between the PVDF layer and the PS layer; the charge storage capacity of these devices is shown in Figure 5e. The transport layer not only gives a better charge storage capacity but also increases the storage depth of the triboelectric charge. As we continue to increase the content of CNTs in the PS transport layer, the total charge quantity increases very slowly (Figure 5f), which means that the amount of stored charge increases more and more slowly when increasing the transport layer's conductivity. This result is also consistent with the calculation above. It is noticed that the stored charge decreases slower and slower along with the increase in carrier mobility or density, as shown in Figure 2 a and b. In summary, the triboelectric charge density can go up 7 times by adding a PS dielectric layer and 11.2 times by building a three-layer structure that includes a PVDF layer, a composite transport layer, and a PS dielectric layer. However, in the previous report, the PVDF nanowire structure can only increase the charge density up to 4.1 times[27] (Figure 6a).

In addition, the charge accumulation process and its decay process over time for the two kinds of TENGs—pure PVDF device (red circles in Figure 6b) and PVDF−PS composite layer device (black squares in Figure 6b)—were tested accordingly. Here, a decay time τ is used to characterize the electron storage capacity for different materials, which means the time it takes for $1/e$ charge to remain. For a pure PVDF device, the decay time τ_{PVDF} is only 22 min. However, when a PS dielectric layer is introduced, the decay time $\tau_{PVDF-PS}$ reaches up to 44 h. This is because most of the triboelectric charges are stored in the PS layer; meanwhile, the abundant trap levels of electrons in PS can bind the flowing electrons effectively.

CONCLUSION

In summary, the transport and storage process of the triboelectric charge in the friction layer was investigated comprehensively. On the basis of the theoretical analysis, we proposed two effective approaches to improve the output performance of the TENG. The first one is to add a PS dielectric layer between the PVDF friction layer and the electrode. The areal density of the total triboelectric charge in the new device is 6 times higher than that in the pure PVDF device. The other approach is to add a transport layer between the friction layer and the dielectric layer or increase the conductivity of the middle layer by introducing a small amount of carbon nanotubes. This method can increase the triboelectric charge yield effectively, and as such, the total charge quantity in the friction layer could be further increased by a factor of 1.6. Aiming at improving the output performance, these two approaches can be widely used to guide the fabrication of TENGs, which provides a solid foundation for TENG research and development.

METHODS

Preparation of the PVDF and PS Solutions. A 2.0 g amount of PVDF was mixed with 8.0 g of *N*,*N*-dimethylformamide (DMF) in a 50 mL triangular flask. The solution was stirred at 60 °C for 3 h and cooled to room temperature. A 3.0 g amount of PS was mixed with 8.0 g of DMF in a 50 mL triangular flask; then it was stirred for 3 h to ensure the dissolution of PS. All reagents were analytically pure and used without any further purification.

Fabrication of TENG Devices. First, to fabricate the negative friction layer part of the TENG, a piece of glass slide with side length of 2.5 cm was prepared as substrate. Then the corresponding size aluminum foil was adhered on the surface of this substrate by double-sided tape. After that, the negative friction layers were prepared on the surface of the aluminum foil by the spin-coating method. By adjusting the spin speed of coating, from 500 rpm to 4000 rpm, the thickness of the friction layer can be controlled easily. For the purpose of facilitating the comparison, all the different negative friciton layers share a single positive friction layer part, which is composed of a glass substrate with a side lengh of 1 cm and a piece of aluminum foil affixed to it.

ASSOCIATED CONTENT

Supporting Information

The Supporting Information is available free of charge on the ACS Publications website at DOI: 10.1021/acsnano.6b02076.

Calculated electron drift process in the friciton layer; figures comparing the triboelectric charge distributions in the friction layers with different parameters (PDF)

AUTHOR INFORMATION

Corresponding Authors

*E-mail: xhma@xidian.edu.cn.
*E-mail: yhao@xidian.edu.cn.

Notes

The authors declare no competing financial interest.

ACKNOWLEDGMENTS

Research was supported by NSFC (Grant No. 61334002) and the Fundamental Research Funds for the Central Universities (Grant Nos. JB161401 and JB161402).

REFERENCES

(1) Fan, F.-R.; Tian, Z.-Q.; Wang, Z. L. Flexible Triboelectric Generator. *Nano Energy* **2012**, *1*, 328−334.
(2) Zou, Y.; Hu, X.; Ma, H.; Li, S. E. Combined State of Charge and State of Health Estimation Over Lithium Ion Battery Cell Cycle Lifespan for Electric Vehicles. *J. Power Sources* **2015**, *273*, 793−803.
(3) Cui, N.; Wu, W.; Zhao, Y.; Bai, S.; Meng, L.; Qin, Y.; Wang, Z. L. Magnetic Force Driven Nanogenerators as a Noncontact Energy Harvester and Sensor. *Nano Lett.* **2012**, *12*, 3701−3705.
(4) Park, K. I.; Son, J. H.; Hwang, G. T.; Jeong, C. K.; Ryu, J.; Koo, M.; Choi, I.; Lee, S. H.; Byun, M.; Wang, Z. L. Highly Efficient, Flexible Piezoelectric PZT Thin Film Nanogenerator on Plastic Substrates. *Adv. Mater.* **2014**, *26*, 2514−2520.
(5) Mao, Y.; Zhao, P.; McConohy, G.; Yang, H.; Tong, Y.; Wang, X. Sponge Like Piezoelectric Polymer Films for Scalable and Integratable Nanogenerators and Self-Powered Electronic Systems. *Adv. Energy Mater.* **2014**, 410.1002/aenm.201301624
(6) Jeong, C. K.; Park, K.-I.; Son, J. H.; Hwang, G.-T.; Lee, S. H.; Park, D. Y.; Lee, H. E.; Lee, H. K.; Byun, M.; Lee, K. J. Self-Powered Fully Flexible Light Emitting System Enabled by Flexible Energy Harvester. *Energy Environ. Sci.* **2014**, *7*, 4035−4043.

DOI: 10.1021/acsnano.6b02076
ACS Nano XXXX, XXX, XXX−XXX

(7) Jeong, C. K.; Park, K. I.; Ryu, J.; Hwang, G. T.; Lee, K. J. Large Area and Flexible Lead Free Nanocomposite Generator Using Alkaline Niobate Particles and Metal Nanorod Filler. *Adv. Funct. Mater.* **2014**, *24*, 2620−2629.
(8) Hwang, G. T.; Park, H.; Lee, J. H.; Oh, S.; Park, K. I.; Byun, M.; Park, H.; Ahn, G.; Jeong, C. K.; No, K. Self-Powered Cardiac Pacemaker Enabled by Flexible Single Crystalline PMN PT Piezoelectric Energy Harvester. *Adv. Mater.* **2014**, *26*, 4880−4887.
(9) Persano, L.; Dagdeviren, C.; Su, Y.; Zhang, Y.; Girardo, S.; Pisignano, D.; Huang, Y.; Rogers, J. A. High Performance Piezoelectric Devices Based on Aligned Arrays of Nanofibers of Poly (vinylidenefluoride-co-trifluoroethylene). *Nat. Commun.* **2013**, *4*, 1633.
(10) Jeong, C. K.; Kim, I.; Park, K.-I.; Oh, M. H.; Paik, H.; Hwang, G.-T.; No, K.; Nam, Y. S.; Lee, K. J. Virus Directed Design of a Flexible BaTiO3 Nanogenerator. *ACS Nano* **2013**, *7*, 11016−11025.
(11) Ramadoss, A.; Saravanakumar, B.; Lee, S. W.; Kim, Y.-S.; Kim, S. J.; Wang, Z. L. Piezoelectric Driven Self Charging Supercapacitor Power Cell. *ACS Nano* **2015**, *9*, 4337−4345.
(12) Zi, Y.; Lin, L.; Wang, J.; Wang, S.; Chen, J.; Fan, X.; Yang, P. K.; Yi, F.; Wang, Z. L. Triboelectric Pyroelectric Piezoelectric Hybrid Cell for High Efficiency Energy Harvesting and Self Powered Sensing. *Adv. Mater.* **2015**, *27*, 2340−2347.
(13) Galchev, T.; McCullagh, J.; Peterson, R.; Najafi, K. Harvesting Traffic-Induced Vibrations for Structural Health Monitoring of Bridges. *J. Micromech. Microeng.* **2011**, *21*, 104005.
(14) Beeby, S. P.; Torah, R.; Tudor, M.; Glynne-Jones, P.; O'Donnell, T.; Saha, C.; Roy, S. A Micro Electromagnetic Generator for Vibration Energy Harvesting. *J. Micromech. Microeng.* **2007**, *17*, 1257.
(15) Mitcheson, P. D.; Green, T. C.; Yeatman, E. M.; Holmes, A. S. Architectures for Vibration Driven Micropower Generators. *J. Microelectromech. Syst.* **2004**, *13*, 429−440.
(16) Tang, W.; Jiang, T.; Fan, F. R.; Yu, A. F.; Zhang, C.; Cao, X.; Wang, Z. L. Liquid Metal Electrode for High Performance Triboelectric Nanogenerator at an Instantaneous Energy Conversion Efficiency of 70.6%. *Adv. Funct. Mater.* **2015**, *25*, 3718.
(17) Lin, L.; Xie, Y.; Niu, S.; Wang, S.; Yang, P.-K.; Wang, Z. L. Robust Triboelectric Nanogenerator Based on Rolling Electrification and Electrostatic Induction at an Instantaneous Energy Conversion Efficiency of∼ 55%. *ACS Nano* **2015**, *9*, 922−930.
(18) Zi, Y.; Lin, L.; Wang, J.; Wang, S.; Chen, J.; Fan, X.; Yang, P. K.; Yi, F.; Wang, Z. L. Triboelectric Pyroelectric Piezoelectric Hybrid Cell for High Efficiency Energy Harvesting and Self Powered Sensing. *Adv. Mater.* **2015**, *27*, 2340−2347.
(19) Su, L.; Zhao, Z. X.; Li, H. Y.; Yuan, J.; Wang, Z. L.; Cao, G. Z.; Zhu, G. High Performance Organolead Halide Perovskite-Based Self-Powered Triboelectric Photodetector. *ACS Nano* **2015**, *9*, 11310−11316.
(20) Li, X.; Yeh, M.-H.; Lin, Z.-H.; Guo, H.; Yang, P.-K.; Wang, J.; Wang, S.; Yu, R.; Zhang, T.; Wang, Z. L. Self-Powered Triboelectric Nanosensor for Microfluidics and Cavity Confined Solution Chemistry. *ACS Nano* **2015**, *9*, 11056−11063.
(21) Wang, S.; Mu, X.; Wang, X.; Gu, A. Y.; Wang, Z. L.; Yang, Y. Elasto-Aerodynamics-Driven Triboelectric Nanogenerator for Scavenging Air Flow Energy. *ACS Nano* **2015**, *9*, 9554−9563.
(22) Cui, N.; Gu, L.; Liu, J.; Bai, S.; Qiu, J.; Fu, J.; Kou, X.; Liu, H.; Qin, Y.; Wang, Z. L. High Performance Sound Driven Triboelectric Nanogenerator for Harvesting Noise Energy. *Nano Energy* **2015**, *15*, 321−328.
(23) Cui, N.; Liu, J.; Gu, L.; Bai, S.; Chen, X.; Qin, Y. Wearable Triboelectric Generator for Powering the Portable Electronic Devices. *ACS Appl. Mater. Interfaces* **2014**, *7*, 18225−18230.
(24) Gu, L.; Cui, N.; Liu, J.; Zheng, Y.; Bai, S.; Qin, Y. Packaged Triboelectric Nanogenerator with High Endurability for Severe Environments. *Nanoscale* **2015**, *7*, 18049−18053.
(25) Jeong, C. K.; Baek, K. M.; Niu, S.; Nam, T. W.; Hur, Y. H.; Park, D. Y.; Hwang, G.-T.; Byun, M.; Wang, Z. L.; Jung, Y. S. Topographically Designed Triboelectric Nanogenerator *via* Block Copolymer Self-Assembly. *Nano Lett.* **2014**, *14*, 7031−7038.
(26) Tang, W.; Zhang, C.; Han, C. B.; Wang, Z. L. Enhancing Output Power of Cylindrical Triboelectric Nanogenerators by Segmentation Design and Multilayer Integration. *Adv. Funct. Mater.* **2014**, *24*, 6684−6690.
(27) Zheng, Y.; Cheng, L.; Yuan, M.; Wang, Z.; Zhang, L.; Qin, Y.; Jing, T. An Electrospun Nanowire Based Triboelectric Nanogenerator and Its Application in a Fully Self-Powered UV Detector. *Nanoscale* **2014**, *6*, 7842−7846.

DOI: 10.1021/acsnano.6b02076
ACS Nano XXXX, XXX, XXX−XXX